Latent heating is required for firestorm plumes to reach the stratosphere

Nathaniel Tarshish[1*], David M. Romps[1,2]

[1] Department of Earth and Planetary Science, University of California, Berkeley, California

[2] Climate and Ecosystem Sciences Division, Lawrence Berkeley National Laboratory, Berkeley, California

July 22, 2022

Abstract

City-wide firestorms produce extreme convective plumes that loft soot into the atmosphere. If emplaced in the stratosphere, soot has long-lasting impacts on global climate. Given the extreme sensible heating from the fire, the importance of additional heating from condensation is unclear and a subject of debate. Analytic plume calculations presented here establish that an idealized dry plume requires a temperature anomaly of at least 60 K at the top of the boundary-layer to remain buoyant up to the cold-point tropopause. Direct numerical and large-eddy simulations indicate that dry firestorm plumes possess temperature anomalies that are less than the requirements for stratospheric ascent by a factor of two or more. In contrast, moist firestorm plumes are shown to reach the stratosphere by tapping into the abundant latent heat present in a moist environment. Latent heating is found to be essential to plume rise, raising doubts about the applicability of past work that neglected moisture.

1 Introduction

The bombings of Hiroshima, Hamburg, and Dresden ignited city-wide fires intense enough to generate their own mesoscale atmospheric circulations (Manins, 1985). These circulations, known as firestorms, act as atmospheric bellows, fanning the fire to even greater intensity by drawing in surrounding air. If triggered, a firestorm is likely to consume all available fuel, and in doing so, firestorms transform cities into vast quantities of soot (Carrier, Fendell, & Feldman, 1985). For context, the Hiroshima firestorm is estimated to have released ten times more energy than the detonated atomic bomb (Aoyama, Kawano, Koizumi, & Okada, 2011; Toon et al., 2007). The fate of firestorm soot has profound consequences for global climate. If lofted by the fire to the stratosphere, soot will block sunlight from reaching the surface and stay lofted for years. Climate models find that megatons of stratospheric soot generate a "nuclear winter" by lowering the global temperature by several degrees Celsius over the following decade (Turco, Toon, Ackerman, Pollack, & Sagan, 1983; Robock, Oman, & Stenchikov, 2007; Mills, Toon, Lee-Taylor, & Robock, 2014; Coupe, Bardeen, Robock, & Toon, 2019; Jägermeyr et al., 2020).

Recent work has aimed to understand what scale of modern nuclear conflict would yield this magnitude of stratospheric soot by studying large eddy simulations of plume ascent (Reisner et al., 2018; Wagman, Lundquist, Tang, Glascoe, & Bader, 2020). A notable difference between two recent studies is that Reisner et al. (2018) ran a dry simulation (i.e., without condensation and latent heating) of the firestorm plume, while Wagman et al. (2020) ran a moist simulation. In ordinary convection, latent heating is the dominant source of buoyancy that lifts deep plumes to the upper atmosphere, but whether latent heating is essential to firestorm plumes is under debate (Robock, Toon, & Bardeen, 2019; Reisner, Koo, Hunke, & Dubey, 2019). Robock et al. (2019) emphasized that large wildfire pyrocumulonimbi are moist, suggesting latent heating's relevance for urban firestorms. On the other hand, Reisner et al. (2019) maintained that wildfire pyrocumulonimbi are exceptional cases, and that extrapolation to firestorms requires further research.

The exceptional formation of a pyrocumulonimbus is known to be dependent on the abundance of environmental moisture (Trentmann et al., 2006; Lareau & Clements, 2016). In observations, the availability of mid-tropospheric moisture is a determining factor of whether a wildfire will generate a deep convective plume (Peterson, Hyer, Campbell, Solbrig, & Fromm, 2017). Stratospheric soot injection from wildfires relies on the buoyancy supplied by condensing this environmental moisture (Trentmann et al., 2006; Peterson et al., 2021).

Differences in geometry and fuel load between wildfires and urban firestorms, however, make dry stratospheric ascent more plausible for a firestorm plume. Urban environments can possess an order of magnitude

---

*Corresponding author: Nathaniel Tarshish, `tarshish@berkeley.edu`

	$\mathcal{H}$ [kW m^{-2}]	R [km]
Hiroshima Aoyama et al. (2011)	20	1
Hamburg Carrier et al. (1985)	70	2
Penner et al. (1986)	10, 90	5
Wagman et al. (2020)	10, 50, 100, 160	2
Small and Heikes (1988)	50	7
Reisner et al. (2018)	$\sim$40	$\sim$2

Table 1: Firestorm sources in the literature.

greater fuel load than dense forest, yielding fire intensities not seen in natural landscapes (Penner, Haselman Jr, & Edwards, 1986; Redfern et al., 2021). Simultaneous ignition of a compact area by a nuclear weapon also yields a fire geometry that contrasts with the perimeter or frontal structure typical of wildfires, and compact areal fires are more favorable to deep convection (Badlan, Sharples, Evans, & McRae, 2021). Therefore, whether moisture is required for stratospheric firestorm plumes remains unclear.

Early modeling efforts addressed this question to two-dimensional simulations and found conflicting results. Small and Heikes (1988) found that a dry firestorm plume lofted soot to the stratosphere. The dry simulations in Penner et al. (1986), on the other hand, run in a similar environment and with comparable fires, became neutrally buoyant before the tropopause. Prior to these numerical models, scaling theories and observation-based models did not emphasize the role of moisture, highlighting instead that the leading determinants of plume height were the magnitude of the fire's heat fluxes and the degree of turbulent mixing with the environment (Manins, 1985; Carrier et al., 1985). In contrast, recent large-eddy simulations in Wagman et al. (2020) found that turning off latent heating lowered the height of soot accumulation from the tropopause at $\sim$15 km down to 8 km, suggesting that moisture indeed plays a fundamental role in soot lofting.

Redfern et al. (2021) also investigated this question by simulating large fires in the same environmental conditions as Reisner et al. (2018), but with the addition of moisture. However, none of the simulations in Redfern et al. (2021) developed into a firestorm. Due to model limitations, the fire source was taken to be a heavy logging slash bed instead of an urban environment (Redfern et al., 2021). In addition, the dynamic fire model did not generate a quasi-steady large area source; instead, all of the fuel in the ignition area was consumed in the first few minutes, and the blaze quickly subsided into a much weaker perimeter fire (Redfern et al., 2021). Absent the mesoscale circulation of a firestorm, and given the fuel load, these results more closely resemble wildfires.

Our lack of a systematic understanding of the effects of latent heating on firestorm plumes presents a challenge to synthesizing these prior findings. It remains unclear under what circumstances, if any, moisture can be relegated to a second-order role. A complicating factor is that firestorm source conditions vary from study to study, as reviewed in Table 1. Fire radii R vary between 1 and 10 km and sensible heat fluxes are generally within the range $\mathcal{H} = 10 - 100$ kW m^{-2}. It is possible that the importance of latent heating is not uniform across this regime.

Here we seek to clarify the importance of latent heating for firestorm soot lofting by investigating the following questions:

- How hot must a plume be at the top of the boundary layer to rise to the stratosphere under dry ascent? (See section 2.)

- Do plumes generated by urban firestorms get this hot? Given heat fluxes in the range of $\mathcal{H} = 10$–100 kW m^{-2}, it may seem intuitive that the plume could be made increasingly hot by enlarging the fire radius R, but we will see that is not true. (See section 3.)

Finally, we probe the importance of latent heating by simulating firestorms in the Reisner et al. (2018) environmental atmosphere with and without moisture in section 4.

2 What plume temperature at the boundary-layer top enables dry ascent to the stratosphere?

We will quantify here the temperature anomaly of a plume entering the troposphere that is required for buoyant ascent to the tropopause without the aid of latent heating.

2.1 Lifting an adiabatic parcel

To facilitate a first estimate of plume rise, we idealize the plume as a parcel and compute the parcel's level of neutral buoyancy under dry, adiabatic ascent. Let T_0' be the plume's temperature anomaly as it enters

the free troposphere at a height of $z_0 \approx 1$ km. As a first pass, we approximate the atmosphere as having a constant lapse rate of $\Gamma = 6$ K km^{-1}. Dry adiabatic ascent sets the parcel's dT/dz to $g/c_p \approx 10$ K km^{-1}, where g is the gravitational constant and c_p is the specific heat capacity of air. For every 1 K of temperature anomaly at z_0, the parcel's level of neutral buoyancy (LNB) rises by $(1\text{K})/(g/c_p - \Gamma) = 250$ m. In the tropical atmosphere, where the tropopause has a height near 15 km, we conclude that an initial temperature anomaly near 60 K is required for dry, adiabatic ascent to the stratosphere.

2.2 Lifting an entraining parcel

We expect that this adiabatic calculation underestimates the initial temperature required for upper atmospheric ascent because we neglected turbulent mixing, which dilutes the plume as it ascends. We approximate this mixing process by assuming there is a characteristic mixing length ℓ over which the parcel's dry static energy s relaxes to the environmental dry static energy s_e such that

$$\frac{ds}{dz} = \frac{(s_e - s)}{\ell} \,. \tag{1}$$

Integrating the dry static energy equation for a plume with initial temperature anomaly T_0' in an environment with constant lapse rate Γ yields

$$T'(z) = e^{-(z-z_0)/\ell} T_0' + \left(1 - e^{-(z-z_0)/\ell}\right)\left(\Gamma - g/c_p\right)\ell \,. \tag{2}$$

Let T_0^* be the temperature anomaly at z_0 required for the plume to reach a level of neutral buoyancy at the tropopause z_t. Setting $T'(z_t) = 0$ and solving for T_0^* yields

$$T_0^* = \left(e^{(z_t - z_0)/\ell} - 1\right)\left(\frac{g}{c_p} - \Gamma\right)\ell \,, \tag{3}$$

which reveals that T_0^* strongly depends on the value of ℓ when $z_t - z_0 \gg \ell$.

To make progress and enable a rough estimation, we adopt the standard Morton, Taylor, and Turner (1956) (hereafter, MTT) entrainment closure, which assumes that the mixing length scales with the horizontal extent of the plume. In other words, the largest vortices, of size comparable to the plume itself, govern the mixing of ambient fluid. Given the plume's radius r, the MTT closure is $\ell = r/(2\alpha)$, where the non-dimensional entrainment constant α has been measured to be near 0.1 in a variety of convection experiments (Tarshish & Romps, 2021; Lecoanet & Jeevanjee, 2019; Stirling & Stratton, 2012; Carazzo, Kaminski, & Tait, 2006). Taking $\alpha = 0.1$ (i.e., $\ell \approx 5r$) and approximating the plume's radius r with the source's radius R provides a simple closure of $\ell = 5R$ that enables analytical computation. For $R = 1\text{-}10$ km (the approximate horizontal extent of a city), plugging into Eqn. 3 yields a first estimation of the temperature required of the entraining plume as it enters the free troposphere if it is to reach the stratosphere. For a tropopause of $z_t = 15$ km, lapse rate $\Gamma = 6$ K km^{-1}, and starting parcel height of $z_0 = 1$ km, Eqn. 3 yields the solid curve shown in Figure 1.

We observe that the importance of mixing for determining the parcel's level of neutral buoyancy strongly depends on the horizontal extent of the underlying heat source. Given a tropopause height ranging from 10-20 km, we expect that plumes with R $\sim$ 10 km are relatively unaffected by entrainment during tropospheric ascent as the characteristic mixing length is 50 km. Plugging this mixing length into Eqn. 3, we find that $T_0^* \approx 66$ K is required to reach the stratosphere, close to the 60 K requirement for the adiabatic parcel. On the other hand, R $\sim$ 1 km plumes possess $\ell \sim 5$ km and go through several e-folding dilutions before reaching the tropopause. In this case, Equation 3 gives $T_0^* \approx 300$ K, five times larger than the adiabatic parcel.

The applicability of this result rests on several idealizations: 1) mixing can be described by a relaxation to environment of the form given in Eqn. 1, 2) the mixing length is accurately described by the MTT closure, and 3) the mixing length can be approximated by taking the plume's radius to be the source's radius. These assumptions can be tested and improved upon by examining the direct numerical simulation (DNS) of a turbulent plume presented in Tarshish and Romps (2021) (hereafter, TR2021). The DNS of TR2021 explicitly resolved the turbulent genesis of a plume by solving the non-dimensionalized Boussinesq equations above a no-slip circular source of buoyancy in an unstratified fluid.

Here we apply the mixing diagnosed in that unstratified simulation to our parcel rising through the stratified troposphere. This application is justified by prior findings that the MTT entrainment hypothesis applies equally well in stratified and unstratified environments: in both cases, experiments find $\alpha \sim 0.1$ (readers are directed to Kaye, 2008, for a review). In stratified flow at the plume's neutrally buoyant top, however, the entrainment model breaks down as the plume spreads horizontally, and the mixing length decouples from the plume's width. Despite this, the MTT model has been broadly successful at predicting LNB heights (Kaye, 2008).
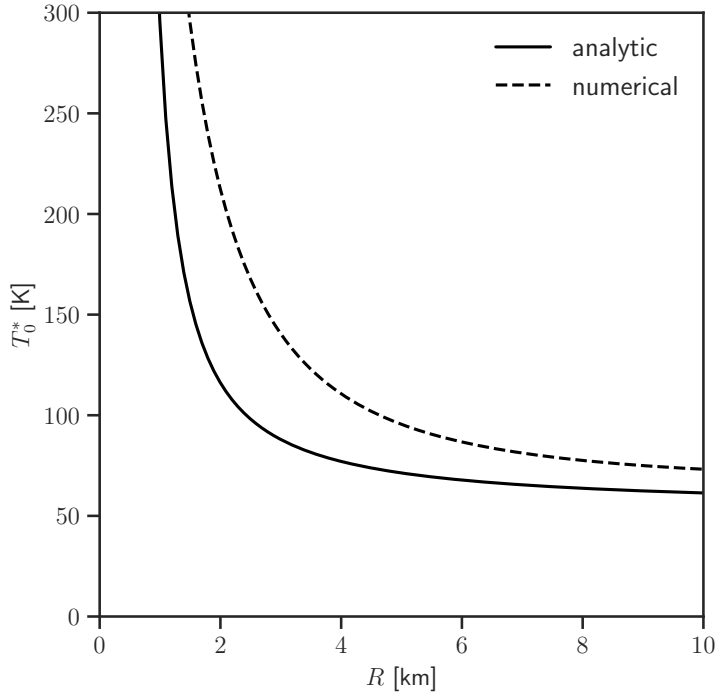
3

Figure 1: The temperature anomaly T_0^* required upon entering the free troposphere ($z_0 = 1$ km) for a dry, entraining parcel to remain buoyant up to the tropopause ($z_t = 15$ km) in an environment with lapse rate $\Gamma = 6$ K km^{-1}. The analytic calculation (solid curve) shows Eqn. 3 evaluated with mixing closure $\ell = 5R$. The numerical solution (dashed curve) applies the mixing trajectory determined from a turbulent plume simulation; in this case, the parcel's dry static energy equation (Eqn. 1) is integrated with the empirical fit to the mixing length $\ell_{\mathrm{DNS}}(z)$ shown in Figure 2.

The plume's Reynolds number in the DNS was 1000, well beneath that of a turbulent plume in Earth's atmosphere. However, as first noted by Scorer (1957), plume entrainment should asymptote to a universal limit that is independent of the Reynolds number once the flow is sufficiently turbulent. By progressively increasing the Reynolds number in two-dimensional simulations, TR2021 estimated that the three-dimensional results examined there were within 20% of this turbulent limit.

To apply the findings here, we first dimensionalize the DNS results by noting that a heat flux of $\mathcal{H}$ (units of kW/m^2) sources buoyancy at a rate $F = g\mathcal{H}/(\rho c_p T_s)$ (units of m^2/s^3), where T_s is the environmental surface-air temperature. Given F and R, dimensional analysis yields the buoyancy profile $b(z) = f(z/R)F^{2/3}R^{-1/3}$, where f is a non-dimensional function that describes how the plume's buoyancy decays with height. The mixing length is computed by differentiating the plume's center-line buoyancy:

$$\ell_{\mathrm{DNS}} = \left(\frac{d\log b}{dz}\right)^{-1}. \tag{4}$$

The TR2021 results for $b(z)$ and ℓ_{DNS} are shown as the solid curves in the middle panels of Figure 2.

To enable future applications and reproducibility, we employ an empirical approximation for $b(z)$ that captures the behavior of the DNS near the surface and then asymptotes to the MTT solution. In terms of $\hat{z} = z/R$, the empirical fit is

$$f_{\mathrm{fit}}(\hat{z}) = f_{\mathrm{MTT}}(\hat{z}) - (2.06 + 14.7(1 - e^{-\hat{z}/0.018}))e^{-\hat{z}/0.56}, \tag{5}$$

where the MTT buoyancy scaling is

$$f_{\mathrm{MTT}}(z) = b_0(\hat{z} - \hat{z}_v)^{-5/3}, \tag{6}$$

and TR2021 measured $b_0 = 31.3$ and $\hat{z}_v = -1.1$. While the DNS and MTT buoyancy curves converge with height, a slight offset persists in Figure 2 up to the sponge layer at $z \approx 7R$, where velocities and buoyancy are damped to achieve a steady state (readers are referred to section 3 of TR2021 for details). The empirical fit defaults to the MTT solution at large heights given the possibility that the DNS is affected by the overlying sponge.

As discussed in TR2021 and shown in Figure 2, the plume exhibits a near-surface layer in which mixing occurs over length-scales much smaller than the plume's radius. This enhanced mixing is driven by a
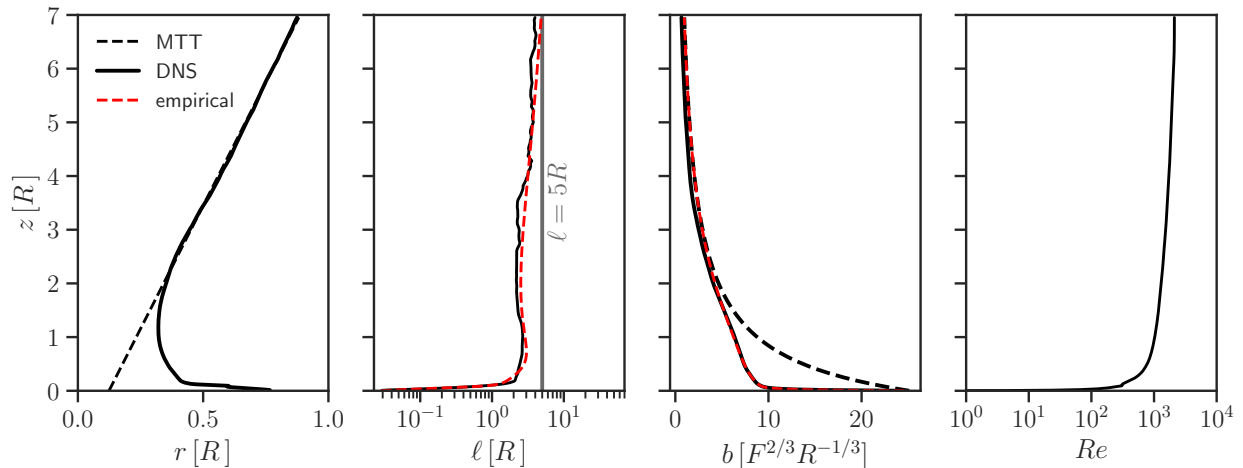
4

Figure 2: Radius, mixing length, buoyancy, and Reynolds number $Re = wr/\nu$ diagnosed in the direct numerical simulation of TR2021 (solid black), along with the MTT scalings (dashed black), the analytic $\ell = 5R$ closure (gray), and the empirical fits to the buoyancy and mixing length (red dashed).

horizontal circulation that is unique to the surface. Above this layer, for $z > 2R$, the plume is well described by the MTT equations, and the plume's radius converges to the analytical solution,

$$r(z) = \frac{6\alpha}{5}\left(z - z_v\right), \tag{7}$$

where z_v denotes the plume's "virtual origin", which TR2021 measured as $z_v \approx -1.1R$. In this MTT region, the diagnosed mixing length closely matches the $\ell = 5r$ parameterization, as shown in the second panel of Figure 2. The plume pinches up near the surface before entering the MTT regime with $r \approx R/3$, which sets the initial mixing length to roughly $\ell_{DNS} \approx 5R/3$. As the plume rises, it widens, eventually coming close to $r = R$ and $\ell_{DNS} \approx 5R$ at $z = 7R$.

We account for this height-dependent mixing by numerically integrating parcel ascent with mixing specified by an empirical fit to the DNS plume. This mixing profile is derived by substituting the empirical fit to the plume's buoyancy (Eqn. 5) into the mixing length definition (Eqn. 4). Both height and the mixing length in the DNS are non-dimensionalized by the fire's radius R. Therefore, specifying R determines a unique vertical profile of mixing between the parcel's origin at $z_0 = 1$ km and the tropopause z_t. Given this mixing profile, we numerically integrate the parcel's dry static energy equation (Eqn. 1) and solve for T_0^*, the parcel's initial temperature that enables positively buoyant ascent up to z_t.

The environment is again specified by $z_t = 15$ km and a lapse rate of $\Gamma = 6$ K km^{-1}. This computation yields the dashed curve in Fig. 1. Comparing the numerical lifting result in Figure 1 to the analytic case, we observe higher initial temperature requirements, consistent with enhanced mixing resulting from the simulated plume's radius being less than the fire's radius.

While the quantitative details differ between the DNS and the analytic calculation, both indicate that if a dry plume enters the free troposphere with a temperature anomaly less than 60 K, then it will fall short of reaching the stratosphere. For plumes with radii less than 3 km, anomalies of hundreds of Kelvins are required to reach the tropopause in the presence of convective entrainment.

2.3 A more realistic environment

The above analysis assumed an idealized environment with a constant lapse rate of $\Gamma = 6$ K/km. Here we show that the findings hold more generally in the more realistic environment of ERA5 reanalysis (Hersbach et al., 2020). We compute the zonal-mean dry static energy over land and average over the time period 2010-2020. This yields the environmental profile $s_e(\phi, z)$, where ϕ is the latitude and z is height. To ease notation, let ϕ be implicit. We solve the entraining dry static energy equation (Eqn. 1) given the plume's initial $s(z_0) = c_p T_0' + s_e(z_0)$, yielding

$$s(z) = e^{-(z-z_0)/\ell}s(z_0) + \frac{e^{-z/\ell}}{\ell}\int_{z_0}^{z} e^{z'/\ell}s_e(z')\,dz', \tag{8}$$

where for simplicity we have assumed that ℓ is constant. Define $T_0^*(z)$ as the *initial temperature anomaly* at the base of the free troposphere (z_0) required of a dry parcel for the parcel to be positively buoyant up
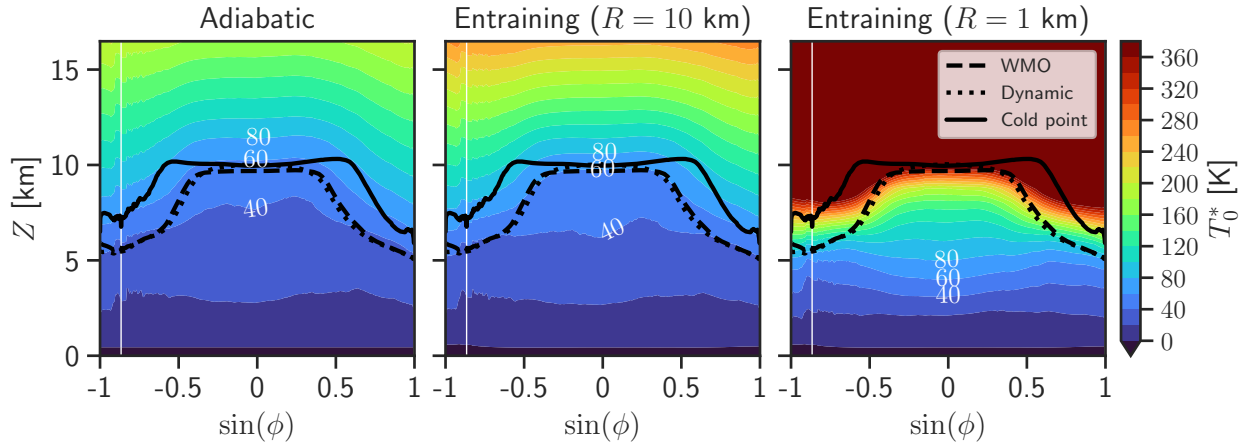
Figure 3: Temperature anomaly $T_0^*(z)$ required of a dry parcel at $z_0 = 1$ km to ascend to a given height under adiabatic motion (left) or entrainment with the $\ell = 5R$ closure (center and right) versus sin of the latitude ϕ. A $R = 10$ km plume (center) has $\ell = 50$ km and thus resembles the adiabatic result in the troposphere. Stronger mixing, with $\ell = 5$ km corresponding to a plume with $R = 1$ km (right), raises the required temperature anomaly by multiples ranging from a factor of two (poles) to six (tropics). The tropopause is shown as defined by the cold point, dynamic definition, and the WMO lapse-rate definition citehoffman. Vertical axis is log-pressure $Z = -H\log(p/p_r)$ with scale height $H = 8$ km and reference pressure $p_r = 1000$ mb.

to z. This can be found by noting that the level of neutral buoyancy occurs where $s = s_e$. Applying this constraint, and solving for $T_0^*(z)$ results in

$$T_0^*(z) = c_p^{-1}\left(s_e(z)e^{(z-z_0)/\ell} - s_e(z_0) - \ell^{-1}e^{z_0/\ell}\int_{z_0}^{z}e^{z'/\ell}s_e(z')\,dz'\right). \tag{9}$$

Applying this formula to the ERA5 data and setting $z_0 = 1$ km yields Figure 3. We illustrate the tropopause layer with the top and bottom contours given by the cold point definition and World Meteorological Organization (WMO) lapse-rate definition, respectively. The WMO tropopause is the lowest level where the absolute value of the temperature lapse rate decreases to 2K/km, or less, with the average lapse rate between this level and all higher levels within 2 km not exceeding 2K/km (Hoffmann & Spang, 2021). The "dynamic" tropopause, a potential vorticity contour of +3.5 PVU, is also shown. The zonal and time average tropopause contours are computed from the ERA5 tropopause dataset (Hoffmann & Spang, 2021).

Consistent with the idealized calculation, we find that reaching the tropical tropopause requires a temperature anomaly of roughly 60 K for an adiabatic parcel. For weak entrainment, corresponding to the plumes with a fire radius of 10 km (thus $l = 50$ km), the entraining and adiabatic results are nearly identical in the troposphere. Decreasing the fire radius to 1 km (implying $l = 5$ km) strands the +60 K plume in the middle of the tropical troposphere; the initial temperature anomaly must be increased to ~ 300 K to reach the tropical stratosphere. At high latitudes, the lower tropopause entails fewer e-folding dilutions for a parcel ascending to the stratosphere, and the temperature requirement is less sensitive to the degree of mixing. A polar adiabatic parcel requires ~ 40 K for stratospheric ascent, and strong mixing ($\ell = 5$ km) roughly doubles this requirement. Given the focus on nuclear winter, the geographic areas of importance here and in prior studies (Wagman et al., 2020; Jägermeyr et al., 2020; Reisner et al., 2018; Mills et al., 2014) are the mid-latitudes and tropics. Not only do these regions contain the majority of urban areas, but stratospheric dynamics raise the risk of nuclear winter; emplacing material in the ascending branch of the stratospheric overturning circulation maximizes the residence time and areal extent (Butchart, 2014).

3   What T_0' can urban firestorms generate?

Now that we have have estimates of the temperature required for dry plumes to reach the stratosphere, we investigate whether firestorms do in fact produce plumes that are hot enough to satisfy these requirements.

3.1   DNS and LES setups

While MTT provides an analytic theory for the far-field plume, there is no analytic theory for the plume near the surface. To provide estimates of the plume's temperature (T_0') in the region of interest, we will rely here on simulations. We will use the DNS of TR2021 as well as large-eddy simulations (LES) that approximate
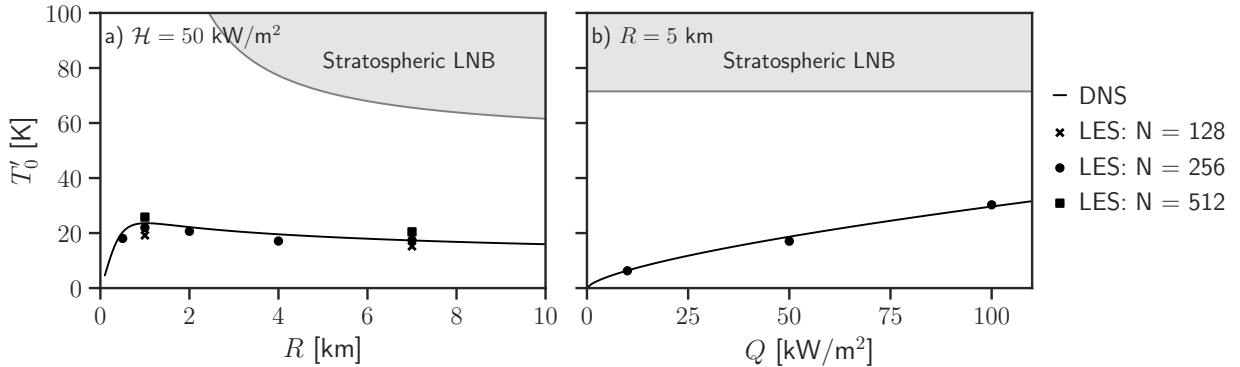
Figure 4: Comparison of the temperature anomaly at 1 km (T_0') for dry plumes in an unstratified fluid given sources with varying radii R (a) and heat fluxes $\mathcal{H}$ (b) in the direct numerical simulation (solid curve) and the large-eddy simulations (scatter). For the $R = 1$ km and 7 km cases, simulations at different resolutions are labeled by the number of grid cells N along each dimension in the uniform grid. The gray area indicates the temperatures that enable stratospheric ascent using, as a conservative estimate, the analytic case in Figure 1.

rather than resolve turbulent dissipation. Each paradigm has its weaknesses (inability to simulate a high Reynolds number with DNS, and limited accuracy of the turbulence closure for LES) so comparing and combining them enables a more robust estimate.

We evaluate the empirical fit to the DNS $b(z)$ plotted in Figure 2 at $z = z_0 = 1$ km to find the initial buoyancy $b(z_0)$ and the temperature anomaly $T_0' = T_e(z_0)b(z_0)/g$ for a range of fire radii and heat fluxes. For $R = 1 - 10$ km and $z_0 = 1$ km, the initial non-dimensional heights are $\hat{z}_0 = z_0/R = 0.1 - 1.0$ in the DNS. Over this height range, the local Reynolds number of the plume increases from roughly 300 to 1000 as shown in the right panel of Figure 2. Therefore, a R = 10 km plume, which has $\hat{z}_0 = 0.1$, is not yet fully turbulent at $z = z_0$ in the simulations. This is a limitation of the model, since plumes in Earth's atmosphere are fully turbulent at $z_0 = 1$ km. Increasing the global Reynolds number from 500 to 10^4 in two-dimensional simulations changes the buoyancy at $\hat{z}_0 = 0.1$ by less than 15% (TR2021, Figure 2). This weak sensitivity to Reynolds number suggests that the three-dimensional DNS may provide a reliable estimate for the atmospheric plume's buoyancy over the height range analyzed here, despite the simulation's semi-turbulent nature close to the surface.

We compare the DNS to LES performed with the fully-compressible, cloud-resolving Das Atmosphärische Modell (DAM) detailed in Romps (2008). Simulations are conducted with an unstratified fluid and a surface temperature of 300 K. One set of simulations has the source radius R varying over [500 m, 1 km, 2 km, 4 km, 7 km] and $\mathcal{H} = 50$ kW m^{-2}. An additional set is run with $\mathcal{H} = [10, 50, 100]$ kW m^{-2} and $R = 5$ km. The setup is configured to match the DNS run described in the appendix of TR2021. Each simulation has a cubic domain with side length $L = 4R$. The flow is damped with Rayleigh drag and Newtonian cooling outside of a half ellipse centered at the surface. (Given the dry lapse rate and surface temperature, the maximum domain height with temperatures above absolute zero is 30 km; given $L = 4R$, this is why the largest R tested is 7 km and not 8 km.)

For each simulation, the chosen heat flux $\mathcal{H}$ specifies the buoyancy flux F, which, along with the fire radius R, gives the characteristic timescale $T = F^{-1/3}R^{2/3}$. Simulations are run for $35T$, steady state is achieved after roughly $10T$, and averages are taken over the last $25T$. The resolution is uniform with $N = 256$ grid cells in each direction. To test for resolution sensitivity, we branch off pairs of additional simulations from the end of the $R = 1$ km and $R = 7$ km simulations. These tests are run for an additional $10T$ with lower resolution ($N = 128$) and higher resolution ($N = 512$), respectively.

3.2   Results

The left panel of Figure 4 shows the results for the DNS and LES cases given varying fire radii. Both the LES and DNS exhibit a global maximum in T_0' (the plume's temperature at $z = 1$ km) for $R \approx 1$ km. Two competing effects result in this maximum at intermediate R. Near the surface, a horizontal circulation of characteristic velocity $U \sim F^{1/3}R^{1/3}$ ventilates the starting layer of buoyancy $B \sim F^{2/3}R^{-1/3}$, a decreasing function of R. However, the buoyancy dilution as the plume rises is set by the mixing length, which is an increasing function of R. The trade-off between maximizing the starting buoyancy (which favors a smaller plume) and preserving the buoyancy during ascent (which favors a larger plume) yields the non-monotonic dependence of T_0' on R. The left panel of Figure 4 shows a maximum magnitude T_0' of approximately 25 K
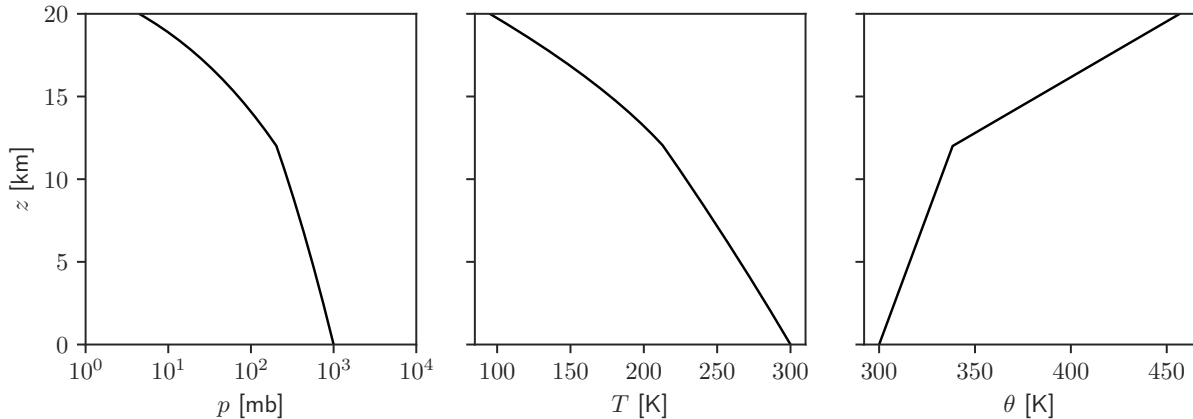
Figure 5: Environmental pressure (left), temperature (center), and potential temperature (right) in the cloud-resolving simulations corresponding to the Reisner et al. (2018) case study.

at $R \approx 1$ km. We estimate the uncertainty in T_0' to be roughly 10 K, the maximum spread between the DNS simulation and the LES simulations, and also roughly the sensitivity of the LES simulations to two doublings in resolution.

Turning to the varying heat flux simulations in the right panel of Figure 4, we observe that the LES estimate is broadly consistent with the DNS scaling $T_0' \propto \mathcal{H}^{2/3}$. Using this scaling, the $T_0' \approx 20$ K result for a $R = 10$ km and $\mathcal{H} = 50$ kW m^{-2} plume in Figure 4 implies that increasing this fire's $\mathcal{H}$ to 100 kW m^{-2} yields a plume with $T_0' \approx 2^{2/3}20 \approx 32$ K. This plume has the largest radius and thus the lowest temperature requirement for stratospheric ascent of any plume in Figure 4. Combined with a heat flux at the upper end of the plausible range for firestorms, this plume has the most favorable properties for stratospheric ascent. Despite these optimal conditions, the plume's temperature anomaly is less than the stratospheric requirement by roughly a factor of two.

Based on this finding, we conclude that firestorm plumes cannot reach the tropical stratosphere under dry ascent. This conclusion points to a clear role for latent heating in lofting soot to the stratosphere. After all, latent heating powers ordinary deep convection to the tropopause despite much less intense boundary-layer sources. The tropical atmosphere is approximately neutrally stable to an ordinary moist entraining plume, with an entrainment rate that is comparable to firestorm plumes and a T_0' that is smaller by one or two orders of magnitude. It therefore stands to reason that a moist firestorm plume would easily ascend to the tropopause in places and times that are already primed to host deep convective storms.

We have applied unstratified simulations to estimate the plume's temperature anomaly at the top of the atmospheric boundary layer. This approach neglected the potential effects of the overlying troposphere on the plume's initial development. The accuracy of this approximation can be estimated by appealing to the characteristic length-scale over which stratification influences the plume,

$$\frac{b}{N^2} = \frac{T_0'}{g/c_p - \Gamma} \sim \frac{30\text{K}}{4\text{K/km}} = 7.5 \text{ km}, \tag{10}$$

where N is the Brunt-Väisälä frequency. Given that b/N^2 is substantially larger than z_0, we expect that the overlying stratification has a limited impact on the boundary-layer ascent. To confirm, we ran an alternate LES simulation (not shown) with the environment set equal to the U.S. standard atmosphere (Minzner, 1977) with a $R = 5$ km and $\mathcal{H} = 50$ kW m^{-2} plume. The difference in T_0' between the stratified and unstratified case is roughly 5 K, suggesting that the unstratified simulations provide valid first-order approximations for our purposes.

4   Case study

The recent study of Reisner et al. (2018) performed dry simulations of a firestorm plume and found that the plume became neutrally buoyant in the lower atmosphere, consistent with the findings here. Given access to moisture, however, we expect that firestorm plumes behave like ordinary deep convective events, which rely on latent heating to reach the upper atmosphere.

We illustrate the importance of latent heating by performing a moist version of the Reisner et al. (2018) simulation. The plume in Reisner et al. (2018) originates from a nuclear blast simulation and fire model, but exact surface fluxes were not reported or archived (personal communication). We estimate from Figure 2 of Reisner et al. (2018) that the actively burning core of the near circular firestorm has $R \approx 2$ km. The
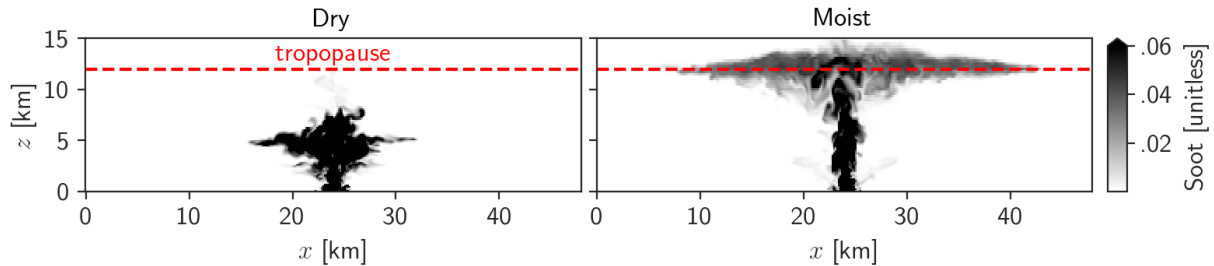
Figure 6: Comparison of moist (left) and dry (right) simulations. Soot cross sections are evaluated at the end of simulations and in the center of the domain. The moist simulation has 70% relative humidity.

average burnable fuel load inside this area is estimated to be 9.1 kg m^{-2} (Robock et al., 2019), which, when combined with an approximate e-folding burn time of 1 hour and the 1.5×10^7 J kg^{-1} energy content of dry wood (Toon et al., 2007), yields a characteristic heat flux of

$$\mathcal{H} = \frac{\left(9.1\text{kg m}^{-2}\right)\left(1.5 \times 10^7 \text{ J kg}^{-1}\right)}{3600 \text{ s}} \approx 40\text{kW m}^{-2}. \qquad (11)$$

This magnitude of heat flux is comparable to the other firestorm cases in Table 1. The environment is taken to be stably stratified and specified by a piece-wise linear potential temperature profile. The lapse rates are estimated from Figure 3 of Reisner et al. (2018) to be $d\theta/dz = 3.2$ K km^{-1} beneath the 12 km tropopause and $d\theta/dz = 14.8$ K km^{-1} above. Figure 5 shows the environmental profile, derived by applying hydrostatic balance above a surface with temperature 300 K and pressure 1000 mb. The temperature lapse rate is near constant in the troposphere and averages to 7.2 K km^{-1}.

The large-eddy simulations presented here are run with a circular fire of radius $R = 2$ km and heat flux $\mathcal{H} = 40$ kW m^2. The heat flux is constant over the hour-long simulation. The environment is initially at rest and specified by the Reisner et al. (2018) setup except for the addition of moisture. We run a dry simulation and a moist simulation with a constant vertical profile of relative humidity of 70%. The DAM domain has horizontal dimensions of 48 km × 48 km and a height of 32 km. The horizontal grid spacing is $\Delta x = \Delta y = 150$ m and the vertical grid spacing increases smoothly from $\Delta z = 10$ m at the surface to $\Delta z = 50$ m at 1 km. For $z > 1$ km, Δz again increases to 100 m at 10 km, and then to 300 m at the domain top. To identify the plume's level of neutral buoyancy, we advect "soot," taken here to be a tracer fixed to 1 throughout the simulation in the bottom grid cells that overlie the surface fire, and initialized as 0 elsewhere. We do not model combustion or actual soot emissions. The soot tracer also has no impact on the moist simulation's microphysics, which is modeled with a six-class Lin-Lord-Krueger scheme (Lin, Farley, & Orville, 1983; Lord, Willoughby, & Piotrowicz, 1984; Krueger, Fu, Liou, & Chin, 1995). Vigorous convection develops within the first few minutes of the simulations, and the vertical soot flux approaches a steady state after roughly fifteen minutes. Soot then begins to accumulate and spread horizontally at the LNB. The large horizontal extent of the domain ensures that the spreading plume top is at least 5 km away from the periodic boundaries at all times.

Figure 6(a) plots a cross section of the soot field at the end of the dry simulation and demonstrates that the dry plume does not reach the upper atmosphere. Soot accumulates instead at ~ 5 km. Our results are consistent with Reisner et al. (2018), who found that their dry plume became neutrally buoyant in the lower atmosphere. Figure 6 in Reisner et al. (2018), in particular, shows a dry LNB of ~ 3 km. The moist simulation, however, rises to the tropopause at 12 km, confirming our expectation: firestorm plumes are able to reach the stratosphere by tapping into the abundant latent heat available in a humid atmosphere.

The surface humidity required to power stratospheric ascent is expected to depend on the environmental stratification. For the particular stratification analyzed here, we explore the sensitivity of the LNB to the abundance of moisture by increasing the relative humidity from 0 to 0.9 by increments of 0.1 in the Reisner et al. (2018) setup. Figure 7 demonstrates how the vertical soot profile depends on the relative humidity. For RH $> .5$, the soot's LNB is at or above the tropopause height of 12 km. As RH decreases, the LNB lowers from the upper troposphere (RH $\sim .5$) to the middle troposphere (RH $\sim .4$) and then demonstrates a secondary lower maxima (RH $= .3$). Only for RH $\leq .2$ does the moist simulation closely resemble the dry simulation. These results suggest that moisture is essential to firestorm plume rise even in relatively dry environments.

While we do not simulate different stratifications, boundary-layer depths, wind shears, relative humidity profiles, or tropopause altitudes, we expect that our central finding—latent heating is required for strato-spheric firestorm ascent—will generally hold in these other environments. This expectation is in part based on the thermodynamic parcel calculations of section 2 and 3. The temperature requirements for dry strato-spheric ascent were found to be fairly uniform across latitudes (Figure 3), suggesting only a weak sensitivity
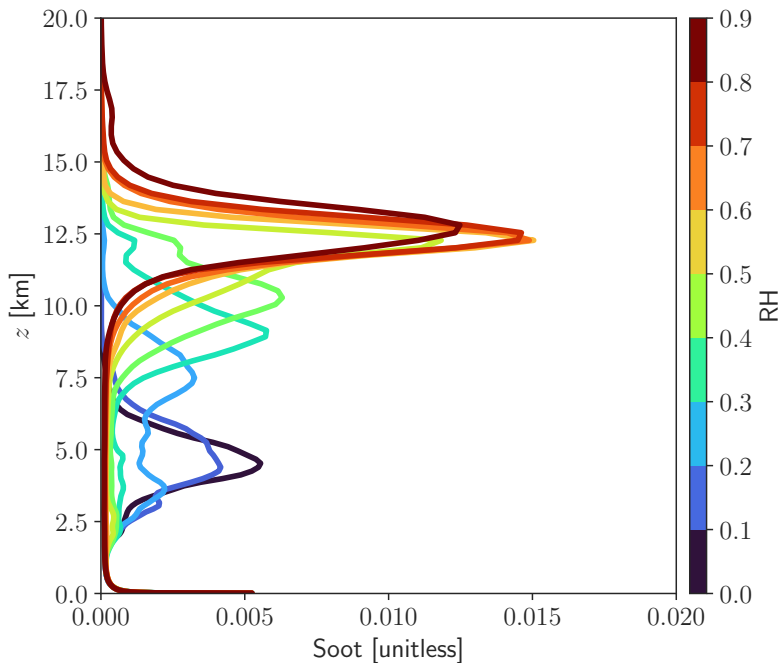
Figure 7: Final vertical profile of soot for simulations with relative humidity (color) varying from 0% to 90% by increments of 10%.

to variations in stratification, boundary-layer depth, and tropopause height. Wind shear is not incorporated into this parcel calculation, but would be expected to increase plume entrainment, and thus further inhibit dry plume ascent. Additional support for the broad applicability of our findings comes from simulations of other firestorms, which showed that dry plumes were unable to reach the stratosphere across a wide array of environmental conditions (Wagman et al., 2020; Redfern et al., 2021).

5   Discussion

Firestorm plumes lift sooty surface air up into the atmosphere. The height at which this soot accumulates determines if the soot is scavenged by precipitation from the lower atmosphere over a few days, or if the soot resides above the weather in the stratosphere for months to years. Soot in the stratosphere dims sunlight at the surface, and megatons of stratospheric soot are thought to yield catastrophic global cooling. The role of latent heating in enabling this stratospheric ascent is a subject of recent debate.

Here, we show that dry ascent is not sufficient to lift firestorm soot to the tropical and mid-latitude stratosphere. We probe dry plume ascent by studying the plume's temperature anomaly T_0' as it enters the free troposphere. Simple lifting calculations indicate that a dry adiabatic plume requires a T_0' of roughly 60 K to reach the tropical tropopause. The accuracy of this adiabatic calculation is shown to depend on the size of the plume's heat source. The plume's radius determines the mixing length ℓ, and mixing becomes a first-order effect if ℓ is comparable to the tropopause height. For firestorm plume's with narrow sources ($R \sim 1$ km), we find that ℓ is a few kilometers. As a result, environmental mixing has a large impact on the ascent, and raises the required temperature anomaly to hundreds of Kelvin.

Both DNS and LES simulations indicate that firestorm plumes with heat sources in the range $\mathcal{H} = 10-100$ kW m^{-2} yield plumes with T_0' at $z_0 = 1$ km in the low tens of Kelvin. We show that this is largely independent of R, and somewhat counter-intuitively, we demonstrate that increasing R beyond a certain value reduces T_0'. A smaller fire radius increases the surface buoyancy, but a larger fire radius lowers the entrainment rate as the plume rises through the boundary layer. An intermediate fire radius has the maximal T_0' due to these competing effects. For subsequent ascent beyond the boundary layer, a larger radius and correspondingly lower entrainment rate is again advantageous for the plume. This entrainment effect dominates such that a larger R is always more advantageous for reaching the stratosphere. Taken together, the simulations indicate that firestorm plumes fall short of the temperature requirements to reach the tropical stratosphere under dry ascent by a factor of at least two.

This claim is compatible with the case study presented here and the prior simulations of Wagman et al. (2020), Reisner et al. (2018), and Penner et al. (1986), who all found dry plume LNBs beneath the stratosphere. The balance of evidence indicates that the stratospheric dry plume of Small and Heikes (1988)

is an outlier. We speculated that the two-dimensional nature of the simulations in Small and Heikes (1988) might be responsible for the discrepancy. To investigate, we ran two-dimensional cases in DAM (not shown), but did not find that the dimensionality had a significant effect on the dry LNB. Therefore, an explanation of the stratospheric dry LNB in Small and Heikes (1988) remains outstanding.

With the addition of moisture, however, we find that firestorm plumes are indeed able to reach the stratosphere. This finding advances the view that firestorm plumes, like ordinary deep convection, reach lofty heights by tapping into the abundant latent heat present in a moist environment. In this view, moisture is a key determinant of plume height, and its essential role was overlooked in prior ascent models (Manins, 1985; Carrier et al., 1985). Our findings indicate that dry simulations should not be used to investigate firestorm plume lofting and cast doubt on the applicability of past research (e.g., Reisner et al., 2018) that neglected latent heating.

A limitation of the theory and simulations presented here is the absence of soot microphysics. Soot aerosols provide cloud condensation nuclei that may alter the drop size distribution and impact auto-conversion. This aerosol effect is expected to invigorate convection (Lee et al., 2020), lofting the plume higher. Coupling soot to microphysics, however, also enables soot to rain out, which could remove much of the soot from the rising plume as suggested in Penner et al. (1986). Given the essential role of moisture in lofting firestorm plumes we identified here, future research should investigate how these second-order microphysical effects impact firestorm soot transport. Another aspect not addressed here and deserving of future study is the radiative lofting of plumes, which has been observed to substantially lift wildfire plume soot for months after the fire (Yu et al., 2019).

Acknowledgments

Availability Statement

Direct numerical simulations were conducted with Dedalus (Burns, Vasil, Oishi, Lecoanet, & Brown, 2020), which is open source and available at `https://dedalus-project.org`. Simulation output and analysis scripts are archived at `https://github.com/nathanieltarshish/latent_firestorms`.

References

Aoyama, M., Kawano, N., Koizumi, T., & Okada, Y. (2011). Estimation of heat, water, and black carbon fluxes during the fire induced by the hiroshima a-bomb. In *Revisit the hiroshima a-bomb with a database latest scientific view on local fallout and black rain* (chap. 5). Hiroshima City.

Badlan, R. L., Sharples, J. J., Evans, J. P., & McRae, R. H. (2021). Factors influencing the development of violent pyroconvection. part ii: fire geometry and intensity. *International journal of wildland fire*, *30*(7), 498–512.

Burns, K. J., Vasil, G. M., Oishi, J. S., Lecoanet, D., & Brown, B. P. (2020). *Dedalus: A flexible framework for numerical simulations with spectral methods* [Software]. doi: 10.1103/PhysRevResearch.2.023068

Butchart, N. (2014). The brewer-dobson circulation. *Reviews of Geophysics*, *52*(2), 157-184. doi: https://doi.org/10.1002/2013RG000448

Carazzo, G., Kaminski, E., & Tait, S. (2006). The route to self-similarity in turbulent jets and plumes. *Journal of Fluid Mechanics*, *547*, 137.

Carrier, G., Fendell, F., & Feldman, P. (1985). Firestorms. *Defense Nuclear Agency Technical Reports*, *DNA-TR-81-102*.

Coupe, J., Bardeen, C. G., Robock, A., & Toon, O. B. (2019). Nuclear winter responses to nuclear war between the united states and russia in the whole atmosphere community climate model version 4 and the goddard institute for space studies modele. *Journal of Geophysical Research: Atmospheres*, *124*(15), 8522–8543.

Hersbach, H., Bell, B., Berrisford, P., Hirahara, S., Horányi, A., Muñoz-Sabater, J., ... Thépaut, J.-N. (2020). The era5 global reanalysis. *Quarterly Journal of the Royal Meteorological Society*, *146*(730), 1999-2049. doi: https://doi.org/10.1002/qj.3803

Hoffmann, L., & Spang, R. (2021). An assessment of tropopause characteristics of the era5 and era-interim meteorological reanalyses. *Atmospheric Chemistry and Physics Discussions*, *2021*, 1–44. doi: 10.5194/acp-2021-961

Jägermeyr, J., Robock, A., Elliott, J., Müller, C., Xia, L., Khabarov, N., ... Rosenzweig, C. (2020). A regional nuclear conflict would compromise global food security. *Proceedings of the National Academy of Sciences*, *117*(13), 7071–7081. doi: 10.1073/pnas.1919049117

Kaye, N. (2008). Turbulent plumes in stratified environments: A review of recent work. *Atmosphere-ocean*, *46*(4), 433–441.

Krueger, S. K., Fu, Q., Liou, K., & Chin, H.-N. S. (1995). Improvements of an ice-phase microphysics parameterization for use in numerical simulations of tropical convection. *Journal of Applied Meteorology and Climatology*, *34*(1), 281–287.

Lareau, N. P., & Clements, C. B. (2016). Environmental controls on pyrocumulus and pyrocumulonimbus initiation and development. *Atmospheric Chemistry and Physics*, *16*(6), 4005–4022.

Lecoanet, D., & Jeevanjee, N. (2019). Entrainment in resolved, dry thermals. *Journal of the Atmospheric Sciences*, *76*(12), 3785-3801. doi: 10.1175/JAS-D-18-0320.1

Lee, S. S., Kablick III, G., Li, Z., Jung, C. H., Choi, Y.-S., Um, J., & Choi, W. J. (2020). Examination of effects of aerosols on a pyrocb and their dependence on fire intensity and aerosol perturbation. *Atmospheric Chemistry and Physics*, *20*(6), 3357–3371.

Lin, Y.-L., Farley, R. D., & Orville, H. D. (1983). Bulk parameterization of the snow field in a cloud model. *Journal of Applied Meteorology and Climatology*, *22*(6), 1065 - 1092. doi: 10.1175/1520-0450(1983)022⟨1065:BPOTSF⟩2.0.CO;2

Lord, S. J., Willoughby, H. E., & Piotrowicz, J. M. (1984). Role of a parameterized ice-phase microphysics in an axisymmetric, nonhydrostatic tropical cyclone model. *Journal of Atmospheric Sciences*, *41*(19), 2836–2848.

Manins, P. (1985). Cloud heights and stratospheric injections resulting from a thermonuclear war. *Atmospheric Environment (1967)*, *19*(8), 1245–1255.

Mills, M. J., Toon, O. B., Lee-Taylor, J., & Robock, A. (2014). Multidecadal global cooling and unprecedented ozone loss following a regional nuclear conflict. *Earth's Future*, *2*(4), 161-176. doi: 10.1002/2013EF000205

Minzner, R. (1977). The 1976 standard atmosphere and its relationship to earlier standards. *Reviews of geophysics*, *15*(3), 375–384.

Morton, B. R., Taylor, G. I., & Turner, J. S. (1956). Turbulent gravitational convection from maintained and instantaneous sources. *Proceedings of the Royal Society of London. Series A. Mathematical and Physical Sciences*, *234*(1196), 1-23. doi: 10.1098/rspa.1956.0011

Penner, J., Haselman Jr, L., & Edwards, L. (1986). Smoke-plume distributions above large-scale fires: Implications for simulations of "nuclear winter". *Journal of Applied Meteorology and Climatology*, *25*(10), 1434–1444.

Peterson, D. A., Fromm, M. D., McRae, R. H., Campbell, J. R., Hyer, E. J., Taha, G., ... DeLand, M. T. (2021). Australia's black summer pyrocumulonimbus super outbreak reveals potential for increasingly extreme stratospheric smoke events. *npj Climate and Atmospheric Science*, *4*(1), 1–16.

Peterson, D. A., Hyer, E. J., Campbell, J. R., Solbrig, J. E., & Fromm, M. D. (2017). A conceptual model for development of intense pyrocumulonimbus in western north america. *Monthly Weather Review*, *145*(6), 2235 - 2255. doi: 10.1175/MWR-D-16-0232.1

Redfern, S., Lundquist, J. K., Toon, O. B., Muñoz-Esparza, D., Bardeen, C. G., & Kosović, B. (2021). Upper troposphere smoke injection from large areal fires. *Journal of Geophysical Research: Atmospheres*, *126*(23). doi: https://doi.org/10.1029/2020JD034332

Reisner, J., D'Angelo, G., Koo, E., Even, W., Hecht, M., Hunke, E., ... Cooley, J. (2018). Climate impact of a regional nuclear weapons exchange: An improved assessment based on detailed source calculations. *Journal of Geophysical Research: Atmospheres*, *123*(5), 2752-2772. doi: 10.1002/2017JD027331

Reisner, J., Koo, E., Hunke, E., & Dubey, M. (2019). Reply to comment by robock et al. on "climate impact of a regional nuclear weapon exchange: An improved assessment based on detailed source calculations". *Journal of Geophysical Research: Atmospheres*, *124*(23), 12959-12962. doi: https://doi.org/10.1029/2019JD031281

Robock, A., Oman, L., & Stenchikov, G. L. (2007). Nuclear winter revisited with a modern climate model and current nuclear arsenals: Still catastrophic consequences. *Journal of Geophysical Research: Atmospheres*, *112*(D13).

Robock, A., Toon, O. B., & Bardeen, C. G. (2019). Comment on a climate impact of a regional nuclear weapon exchange: An improved assessment based on detailed source calculations by reisner et al. *Journal of Geophysical Research: Atmospheres*, *124*(23), 12953-12958. doi: https://doi.org/10.1029/2019JD030777

Romps, D. M. (2008). The dry-entropy budget of a moist atmosphere. *Journal of the Atmospheric Sciences*, *65*(12), 3779–3799.

Scorer, R. S. (1957). Experiments on convection of isolated masses of buoyant fluid. *Journal of Fluid Mechanics*, *2*(6), 583–594. doi: 10.1017/S0022112057000397

Small, R. D., & Heikes, K. E. (1988). Early cloud formation by large area fires. *Journal of Applied Meteorology and Climatology*, *27*(5), 654 - 663.

Stirling, A. J., & Stratton, R. A. (2012). Entrainment processes in the diurnal cycle of deep convection over land. *Quarterly Journal of the Royal Meteorological Society*.

Tarshish, N., & Romps, D. M. (2021). A closure for the virtual origin of turbulent plumes. *Journal of the Atmospheric Sciences*. doi: 10.1175/JAS-D-21-0096.1

Toon, O. B., Turco, R. P., Robock, A., Bardeen, C., Oman, L., & Stenchikov, G. L. (2007). Atmospheric effects and societal consequences of regional scale nuclear conflicts and acts of individual nuclear terrorism. *Atmospheric Chemistry and Physics*, *7*(8), 1973–2002. doi: 10.5194/acp-7-1973-2007

Trentmann, J., Luderer, G., Winterrath, T., Fromm, M. D., Servranckx, R., Textor, C., ... Andreae, M. O. (2006). Modeling of biomass smoke injection into the lower stratosphere by a large forest fire (part i): reference simulation. *Atmospheric Chemistry and Physics*, *6*(12), 5247–5260. doi: 10.5194/acp-6-5247-2006

Turco, R. P., Toon, O. B., Ackerman, T. P., Pollack, J. B., & Sagan, C. (1983). Nuclear winter: Global consequences of multiple nuclear explosions. *Science*, *222*(4630), 1283–1292.

Wagman, B. M., Lundquist, K. A., Tang, Q., Glascoe, L. G., & Bader, D. C. (2020). Examining the climate effects of a regional nuclear weapons exchange using a multiscale atmospheric modeling approach. *Journal of Geophysical Research: Atmospheres*, *125*(24).

Yu, P., Toon, O. B., Bardeen, C. G., Zhu, Y., Rosenlof, K. H., Portmann, R. W., ... Robock, A. (2019). Black carbon lofts wildfire smoke high into the stratosphere to form a persistent plume. *Science*, *365*(6453), 587-590. doi: 10.1126/science.aax1748